Robust Automatic C-arm Calibration for Fluoroscopy-based Navigation: a Practical Approach *

H. Livyatan, Z. Yaniv, and L. Joskowicz

School of Computer Science and Engineering
The Hebrew University of Jerusalem, Jerusalem 91904, Israel.
Email: {livyatan,zivy,josko}@cs.huji.ac.il

Abstract. This paper presents a new on-line automatic X-ray fluoroscopic C-arm calibration method for intraoperative use. C-arm calibration is an essential prerequisite for accurate X-ray fluoroscopy-based navigation and image-based registration. Our method utilizes a custom-designed calibration ring with a two-plane pattern of fiducials that attaches to the C-arm image intensifier, and an on-line calibration algorithm. The algorithm is robust, fully automatic, and works with images containing anatomy and surgical instruments which cause fiducial occlusions. It consists of three steps: fiducial localization, distortion correction, and camera calibration. Our experimental results show submillimetric accuracy for calibration and tip localization with occluded fiducials.

1 Introduction

Research in computer-aided surgery (CAS) has focused on developing X-ray fluoroscopy-based systems to improve the surgeons' hand/eye coordination, to improve the accuracy and repeatability of surgical gestures, to reduce cumulative radiation, and to shorten surgery times. Fluoroscopy-based CAS systems include virtual fluoroscopy navigation, CT-based navigation with 2D/3D image registration, and tool and robot localization [6]. An essential prerequisite in all these systems is the calibration of the X-ray fluoroscopic unit.

Recently, many works have focused on X-ray fluoroscopy calibration both in academia [1, 4, 8, 9, 12, 13] and in industry (FluoroNav, Medtronic Sofamor Danek, USA, and SurgiGATE AG, Medivision, Switzerland). These works show that the localization error is significant (up to 5mm in older units) and that the calibration parameters are orientation dependent, so they must be corrected independently for each orientation. Two approaches have been proposed: an off-line approach [1, 12] and an on-line approach [4, 8, 9, 13].

In the off-line approach, the calibration parameters are computed for a fixed set of C-arm orientations before the surgery starts. In the on-line approach, the

* This research was supported in part by a grant from the IZMEL Consortium on Image-Guided Therapy, Israel Ministry of Industry and Trade. We thank Neil Glossop from Traxtal Technologies for the design and manufacturing of the phantom.

parameters are computed anew for each image during surgery. The off-line approach allows for larger calibration phantoms, denser grids, and produces images which are simpler to analyze, since only fiducials are present in the image. However, it requires a separate calibration step performed by an X-ray technician and limits the viewing angles that can be used. The on-line approach does not have these limitations but requires a more sophisticated image processing algorithm. It presents trade-offs between calibration phantom size, grid density, and accessibility on the one hand, and robustness and accuracy on the other. The later critically depend on the precise localization of fiducials centers and their pattern. Published methods only address these problems partially.

2 Materials and Methods

We have developed a fully automatic on-line X-ray fluoroscopic image calibration method that includes a calibration phantom and a calibration algorithm. The phantom and the algorithm were developed after considering and experimenting with the trade-offs of on-line calibration, and with special attention to robustness and accuracy in actual surgical situations in which X-ray images include anatomy, implants, and surgical tools that occlude some of the calibration fiducials. The algorithm detects when the calibration cannot be performed accurately due to poor image quality or too many occluded fiducials.

We co-designed with Traxtal Technologies (Toronto, Canada) the FluoroTrax, an optically tracked on-line C-arm calibration phantom. The phantom consists of a ring frame on which 32 LEDs for optical tracking are mounted and two parallel radiolucent plates 76mm apart with 120 embedded fiducial steel balls of two diameters (2mm and 3mm). The small fiducials are arranged in a regular Cartesian grid pattern with 20mm spacing between their centers. The big fiducials (21 of them) are all in the upper plate and form a U-shaped pattern consisting of a pair of parallel lines intersected by an orthogonal line. The ring frame attaches with three fast-release clamps to the C-arm's image intensifier (in our case, a Phillips BV29 unit with a 9" field of view). The phantom is isolated from the sterile surgical field by wrapping it with a transparent plastic sheet.

The three-step calibration algorithm computes the calibration parameters from a single X-ray image and from a spatial model of the fiducial centers. First, it locates the fiducials and their patterns and matches them to the model. It then computes the calibration parameters and the distortion correction.

2.1 Fiducial and calibration pattern localization

Accurate and robust localization of the fiducials and their patterns is the most important step of the calibration process, since all parameters critically depend on it. The localization consists of finding the fiducial centers in the X-ray fluoroscopic image and pairing them with the corresponding fiducial centers in the model. To be practical, this step must be real-time, fully automatic, and take

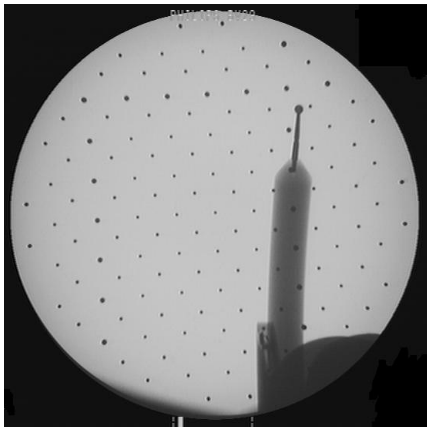

(a) Original image

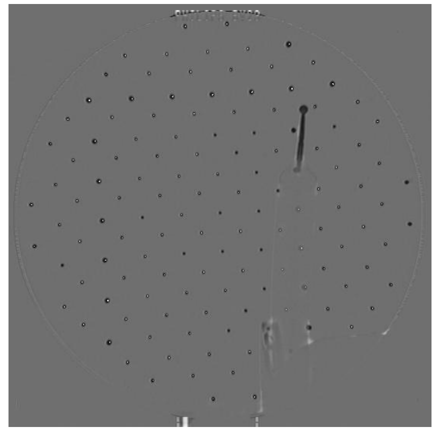

(b) After subtraction and NCC thresholding

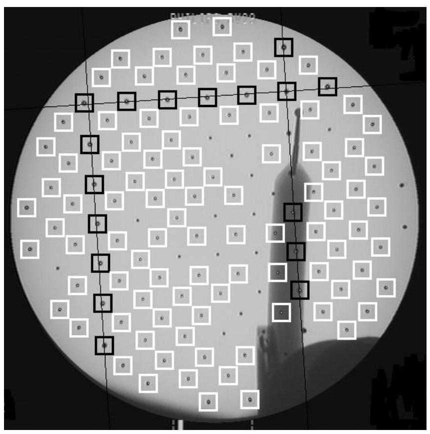

(c) U-shaped pattern localization

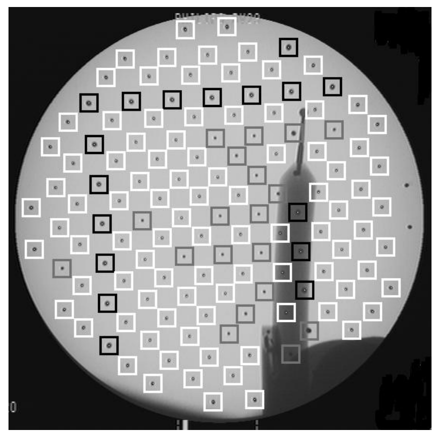

(d) Missing fiducials localization

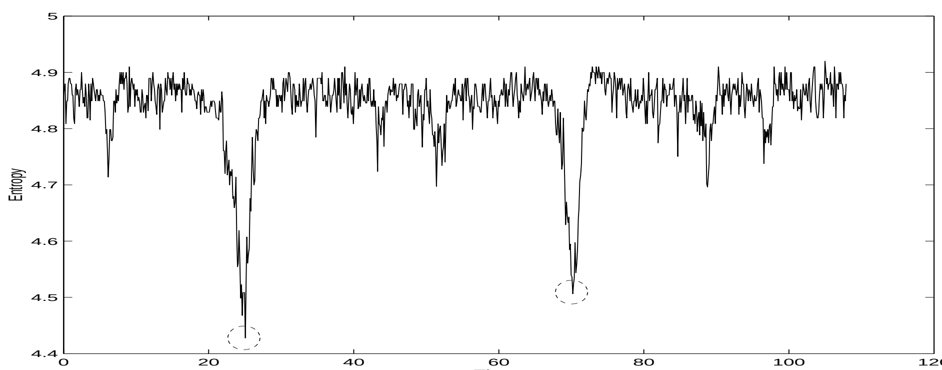

(e) Entropy of the grid point projections as a function of their orientation.

Fig. 1. Illustration of the fiducial and calibration pattern localization step. White dots show fiducial center. Fiducials inside black boxes are U-shaped pattern fiducials, inside white boxes are grid pattern fiducials, and inside gray boxes are recovered fiducials.

into account local intensity variations across the image. Fig. 1 illustrates the process.

The algorithm finds the fiducials and their centers and then matches the U-shaped and the grid patterns to them. The search for fiducials proceeds as follows. First, the algorithm subtracts from the original X-ray fluoroscopic image a background image of it from which the fiducials have been morphologically removed. The background image is computed by performing a median filter on the original image with a square kernel whose size is the small fiducials diameter [9]. Since the gray level values of the pixels occupied by the fiducials in the original image are lower than that of the background, the gray level values at those pixels will be negative after the subtraction. Those pixels are candidates for fiducial locations (Fig. 1(b)). To determine which pixels are fiducial pixels, the algorithm computes the Normalized Cross Correlation (NCC) values with two circle templates (one for big and one for small fiducials) at those pixels. Candidate pixels whose NCC value is greater than a predetermined threshold value are fiducial pixels. Those pixels form clusters of candidate fiducial center locations. To find the actual fiducial centers, the algorithm segments out each fiducial with a local gray-level threshold computed in the vicinity of the candidate fiducial pixels. For each fiducial cluster, it finds the pixel with the highest NCC value. Two concentric squares are centered at this pixel. The pixel gray-level mode value inside the inner square is defined as the fiducial gray-level value. The pixel gray-level mode value inside the outer square is defined as the background gray-level value. The average of these two defines the local fiducial segmentation threshold. The fiducial center is the weighted center of gravity of the resulting segmentation.

To find the U-shaped pattern which determines the coordinate frame of the phantom, the algorithm first finds the orientation of the phantom grid by rotating the fiducial centers c_i by an angle θ_j and projecting them on the horizontal axis, obtaining a value $x_i(\theta_j)$. The algorithm computes the histogram entropy of the projected values $\{x_i(\theta_j)\}$ for uniformly sampled angles θ_j:

$$entropy(\theta_j) = -\sum_{i=1}^{n} p(x_i(\theta_j)) \log_2 p(x_i(\theta_j))$$

where $p(x)$ is the probability of x in its histogram. The angle θ_j which yields the lowest entropy corresponds to the grid orientation.

Fig. 1(e) shows an example of the entropy graph for a range of angles. Note that the graph has two very similar minimum values. The first minimum corresponds to grid lines, and the second corresponds to grid diagonals. Due to sampling and numerical inaccuracies, the two values might be interchanged, leading to the wrong conclusion. The algorithm determines which one of the two minima corresponds to grid lines by comparing the distances between the lines in both orientations and choosing the smallest, since the distance between diagonals is smaller than the distance between grid lines.

The algorithm proceeds to identify the fiducials forming the U-shaped pattern by assigning a weight to each fiducial according to its NCC and gray-level pixel

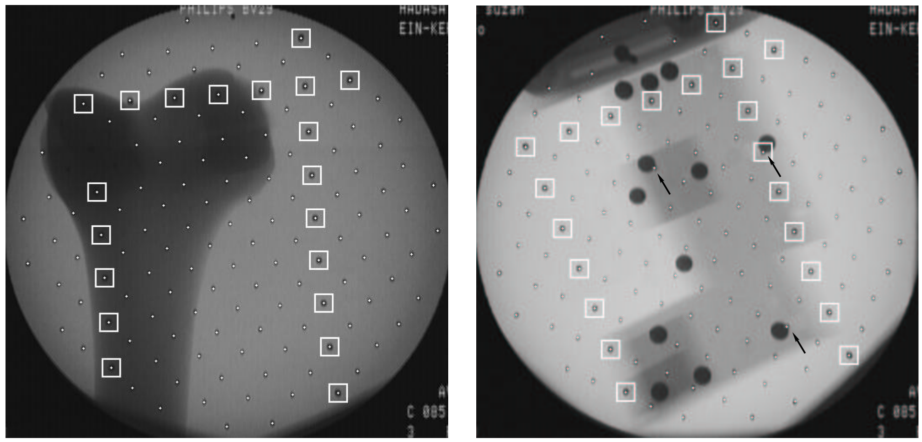

Fig. 2. Robust fiducial and U-shaped pattern localization on two X-ray fluoroscopic images. The left image illustrates robust pattern detection with missing fiducials (at the top left of the image). The right image illustrates robust fiducial detection with fiducial occlusions (indicated by the arrows in the image).

values. The weights define two clusters, for the small and big fiducials. The two parallel lines and the orthogonal line with the largest number of big fiducials are the U-shaped pattern (Fig. 1(c)).

Finally, the algorithm attempts to recover additional fiducials at grid intersections where no fiducials were found by repeating the steps above with a lower threshold on the NCC value (Fig. 1(d)). Fig. 2 illustrates fiducial and pattern localization on two realistic images.

2.2 Camera calibration

We model the C-arm as a pin-hole camera with distortion [1, 4, 12]. Camera calibration consists of computing intrinsic (focal length, image center coordinates, horizontal and vertical pixel scales) and extrinsic (spatial position and orientation of the camera) camera parameters. We implemented two well known camera calibration methods: Faugeras' method [2] and the linear method described in [3, 11]. Faugeras' method requires at least six points in general position, while the linear method requires nine points on two planes. Both methods are applicable to the FluoroTrax, which has more points. As we will see next, both algorithms are experimentally comparable. The calibration result is significantly dependent on the fiducial center locations passed to either calibration method. Using fiducial center locations as found in the distorted image will lead to incorrect results. A simple solution is to use only fiducials central to the image where the distortion is minimal. We offer a more complex solution that leads to better results. In order to calculate the locations of the dewarped fiducial centers belonging to the upper plate of FluoroTrax, we need to find the correct location of its dewarped grid. The center of the grid might be computed by intersecting the grid lines passing through it. The grid interval is a predefined constant and should not be computed, due to the adjacency of the upper plate to the image intensifier. The locations of the dewarped fiducial centers belonging to the lower plate are computed by the two-pass mesh warping algorithm described in [10], based on the correction of the fiducial centers in the upper plate. These dewarped fiducial centers enable proper calibration.

2.3 Distortion correction

Distortion correction consists of computing a dewarping function that inputs a point in the image and returns its corrected location. The dewarping function is computed by comparing the locations of the fiducial centers with their spatial locations projected by the calibrated camera.

The dewarping function can be computed for the entire image (globally) or for portions of it (locally). In the global approach, the dewarping function parameters are computed by fitting a surface, such as a bi-cubic polynomial, to the fiducial centers [4, 13]. In the local approach, each grid square defined by four contiguous fiducials defines a region with its own dewarping function [8, 12]. The local approach requires that all fiducial centers be detected, which is only realistic in off-line calibration. The global approach is better suited for on-line calibration since we can fit a surface to the fiducial centers even when some are missing, although their absence degrades the accuracy. We fit a cubic B-spline to each horizontal and vertical line of fiducial centers and then apply the two-pass mesh warping algorithm described in [10].

3 Experimental Results

We conducted three sets of experiments to evaluate the robustness and accuracy of our calibration method. The first quantifies the accuracy of the distortion correction process. The second quantifies the sensitivity of the calibration process to missing fiducials. The third quantifies the accuracy of the entire process and compares the two camera calibration methods discussed above.

To quantify the accuracy of the distortion correction step, we attach the FluoroTraX to the image intensifier, acquire a reference image, rotate the FluoroTraX by an unknown amount around the image intensifier cylinder, and acquire a test image. We compute the dewarping function from the reference image and apply it to the test image. We then compute the distance between the expected location of the fiducial centers and their corrected location in the test image. The following table summarizes the results (values are in pixels, millimeters in parenthesis):

Image	number of points	Maximum	Minimum	Mean	Std. Dev.
1	97	1.96 (0.84)	0.06 (0.03)	0.83 (0.36)	0.45 (0.19)
2	101	2.23 (0.96)	0.04 (0.02)	0.83 (0.36)	0.50 (0.21)
3	97	2.39 (1.03)	0.16 (0.07)	0.95 (0.41)	0.50 (0.21)
4	98	1.99 (0.86)	0.06 (0.03)	0.77 (0.33)	0.49 (0.21)
Average	98	2.14 (0.36)	0.08 (0.03)	0.84 (0.36)	0.48 (0.21)

To quantify the sensitivity of the calibration process on missing fiducials, we manually removed fiducials from the images and recorded the calibration parameters values. The following table summarizes the results.

Number of points	focal length (mm)	focal point (mm)	image center (pixels)	pixel size (mm)
61	885.55	5.42, -0.07, 922.55	376.24, 288.02	0.43, 0.43
56	883.48	6.15, 0.46, 920.48	374.57, 286.62	0.43, 0.43
51	864.56	6.02, 1.05, 901.56	374.93, 285.29	0.43, 0.43
46	865.63	6.43, 1.02, 902.63	373.88, 285.34	0.43, 0.43
41	853.65	5.77, 1.90, 890.65	375.45, 283.33	0.43, 0.43
Max. diff.	31.9	0.66, 2.06, 31.80	2.36, 4.69	0.00, 0.00
%	3.6%	10.3%	10.6%	0.0%

Note that although the indiviudal parameter variations can be up to 10% as the number of fiducial points decreases, the values are still meaningful even when only 41 out of 120 fiducials are detected.

To quantify the accuracy of the entire process, we compare the tracked position of a tool tip with its location in the X-ray image. We place an optically tracked pointing device with a spherical tip (Polaris, Northern Digital, Ontario, Canada) in the C-arm field of view and compute two distances. The first is the distance between the tip location in the image and its projection according to its spatial location given by the tracking system. This distance quantifies the accuracy of fluoroscopy-based navigation. The second is the distance between the ray defined by the camera focal point and the tip center in the image and the tip center spatial location given by the tracking system. This distance quantifies the accuracy of 2D/3D image-based registration. We compute both distances twice, with the linear method [3, 11] and with Faugeras' calibration method [2]. Fig. 3 shows the results of the first distance. The following table summarizes the results (all measurements are in millimeters, with standard deviation in parenthesis).

Image	1. Distance in image plane		2. Distance between ray and tip	
1	linear method	Faugeras' method	linear method	Faugeras' method
2	1.07	1.13	0.8	0.82
3	1.38	1.39	1.0	0.98
4	0.80	0.86	0.52	0.54
5	0.93	0.89	0.45	0.41
6	1.01	1.02	0.76	0.75
7	0.56	0.57	0.37	0.37
8	1.04	1.05	0.63	0.62
9	0.63	0.59	0.30	0.27
Average	0.92 (0.26)	0.93 (0.27)	0.60 (0.23)	0.59 (0.23)

These results indicate that both camera calibration algorithms are comparable and that accuracy is sufficient for X-ray fluoroscopy-based procedures.

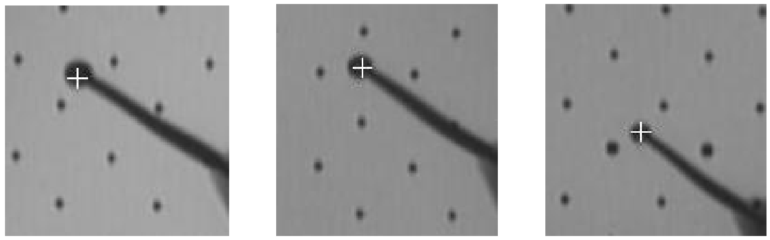

Fig. 3. Projection of tracked pointer tip location onto the X-ray image after calibration.

4 Discussion and Conclusions

We have presented a new on-line X-ray fluoroscopic C-arm calibration method for intraoperative use. The method is robust, fully automatic, and works with images in which calibration fiducials are occluded by anatomy and surgical instruments. Our experimental results show that: (1) the on-line dewarping accuracy, while not as accurate as the off-line one in [12] (405 fiducials, $mean = 0.10$mm, $\sigma = 0.06$mm, $min = 0.01$mm, and $max = 0.20$mm. vs. 120 fiducials $mean = 0.36$mm $\sigma = 0.21$mm, $min = 0.03$mm, and $max = 0.36$mm), it is still very good and is not the main contributor of the calibration inaccuracy; (2) the calibration parameters are very sensitive to the fiducial center locations and to how many are used to compute the calibration parameters, and; (3) the accuracy of the entire calibration process is below a millimeter, with either the Faugeras [2] or the linear camera calibration [3, 11] methods, which yield very similar results.

We are currently using the calibration method in two orthopaedic applications: 2D/3D image-based registration for fracture reduction [5] and image-based robot positioning for distal locking [7]. We are also evaluating the in-vitro accuracy and robustness of the entire X-ray image-based registration.

References

1. Brack C., Burgkart R., Czopf A., Gotte H., "Accurate X-Ray-Based Navigation in Computer-Assisted Orthopedic Surgery" *Proc. 12th Int. Symp. on Computer Assisted Radiology and Surgery*, H.U. Lemke *et al.* eds, 1998.
2. Faugeras O., *3D Computer Vision: A Geometric Viewpoint*, MIT Press, 1993.
3. Gremban K., Thorpe C., Kanade T., "Geometric Camera Calibration Using a System of Linear Equations", *Proc. of IEEE Int. Conf. on Robotics and Automation*, 1988.
4. Hofstetter R., Slomczykowski M., Sati M., Nolte LP., "Fluoroscopy as an Imaging Means for Computer-Assisted Surgical Navigation", *Comp. Aided Surgery* **4**(2), 1999.
5. Joskowicz L., Milgrom C., Simkin A. et al. "FRACAS: A System for Computer-Aided Image-Guided Long Bone Fracture Surgery", *Comp. Aided Surgery* **3**(6), 1999.
6. Joskowicz L., "Fluoroscopy-Based Navigation in Computer-Aided Orthopedic Surgery", *Proc. of the IFAC Conf. on Mechatronic Systems*, 2000.

7. Joskowicz, L., Milgrom, C., Shoham, M., Yaniv, Z., and Simkin, A., "Robot-Guided Long Bone Intramedullary Distal Locking: Concept and Preliminary Results", *Proc of the 3rd Int. Symposium on Robotics and Automation*, Mexico, Sept. 2002.
8. Tang S.Y.T., "Calibration and Point-Based Registration of Fluoroscopic Images", MSc Thesis, Dept. of Computer Science, Queen's Univ., Ontario, Canada, 1999.
9. Tate P.M., Lachine V., Fu L. et. al, "Performance and Robustness of Automatic Fluoroscopic Image Calibration in a new Computer Assisted Surgery System", *Proc. of Medical Image Computing and Computer Assisted Intervention*, 2001.
10. Wolberg G., *Digital Image Warping*, IEEE Press, 1990.
11. Yakimovsky Y., Cunningham R., "A system for extracting 3D measurements from a stereo pair of TV cameras", *Computer Graphics and Image Processing* 1978.
12. Yaniv Z., Joskowicz L., Simkin A., Garza-Jinich M., Milgrom C., "Fluoroscopic Image Processing for Computer-Aided Orthopedic Surgery" *1st Int. Conf. on Medical Computing and Computer-Assisted Intervention*, Lecture Notes in Computer Science 1496, Elsevier, Wells et al eds. 1998.
13. Yao J., Taylor R.H., Goldberg R.P., "A C-Arm Fluoroscopy-Guided Progressive Cut Refinement Strategy Using a Surgical Robot", *Comp. Aided Surgery* **5**(6), 2000.